metals

MDPI

Article

Decorative Multi-Walled Carbon Nanotubes by ZnO: Synthesis, Characterization, and Potent Anti-Toxoplasmosis Activity

Jehan Y. Al-Humaidi [1], Mohamed Hagar [2], Basant A. Bakr [3], Bassma H. Elwakil [4,*], Esraa Abdelhamid Moneer [4] and Mostafa El-Khatib [5]

[1] Department of Chemistry, College of Science, Princess Nourah Bint Abdulrahman University, P.O. Box 84428, Riyadh 11671, Saudi Arabia; Jyalhamidi@pnu.edu.sa
[2] Department of Chemistry, Faculty of Science, Alexandria University, Alexandria 21321, Egypt; mohamedhaggar@gmail.com
[3] Department of Zoology, Faculty of Science, Alexandria University, Alexandria 21321, Egypt; bassant.kamal@pua.edu.eg
[4] Department of Medical Laboratory Technology, Faculty of Applied Health Sciences Technology, Pharos University in Alexandria, Alexandria 21526, Egypt; esraa.moneer@pua.edu.eg
[5] Basic Sciences Department, Faculty of Engineering, Pharos University in Alexandria, Alexandria 21526, Egypt; mostafa.elkhatib@pua.edu.eg
* Correspondence: bassma.hassan@pua.edu.eg

Abstract: Toxoplasmosis may become a fatal disease in immunodeficient, diabetic patients, pregnant women, and infants. Hence, the diligent search for new effective treatment is among the major concerns worldwide. The well-dispersed multi-walled carbon nanotubes lined with ZnO (ZnO-MWCNT), graphene oxide (GO-NPs), and zinc oxide (ZnO-NPs) were successfully synthesized through rapid and facile hydrothermal arc discharge technique (HTADT). The antiparasitic effects of ZnO-NPs, GO-NPs, and ZnO-MWCNT were investigated in mice infected with *Toxoplasma gondii*. The percent of tachyzoites reduction were detected. The observed results demonstrated that ZnO-MWCNT revealed a significant reduction in the parasite count reached 61% in brain tissues, followed by liver (52%), then spleen (45%). The assessments of antiparasitic, inflammatory, and anti-inflammatory cytokines confirmed the superior activity of ZnO-MWCNT as antiparasitic agent, which paves the way for the employment of ZnO-MWCNT as a treatment for the acute RH strain of *T. gondii* infection in vivo.

Keywords: arc discharge; nanostructures; ZnO-MWCNT; antiparasitic; *Toxoplasma gondii*; in vivo study; immunological studies

check for updates

Citation: Al-Humaidi, J.Y.; Hagar, M.; Bakr, B.A.; Elwakil, B.H.; Moneer, E.A.; El-Khatib, M. Decorative Multi-Walled Carbon Nanotubes by ZnO: Synthesis, Characterization, and Potent Anti-Toxoplasmosis Activity. *Metals* **2022**, *12*, 1246. https://doi.org/10.3390/met12081246

Academic Editor: Manuel Aureliano

Received: 27 June 2022
Accepted: 21 July 2022
Published: 25 July 2022

Publisher's Note: MDPI stays neutral with regard to jurisdictional claims in published maps and institutional affiliations.

Copyright: © 2022 by the authors. Licensee MDPI, Basel, Switzerland. This article is an open access article distributed under the terms and conditions of the Creative Commons Attribution (CC BY) license (https://creativecommons.org/licenses/by/4.0/).

1. Introduction

Over the past decade, carbon nanostructures have been used in a medical of field due to controlled- and sustained-release properties, subcellular size, and biocompatibility with tissue and cells, which is why CNTs have become one of the major achievements in the field of nanotechnology [1–3]. According to several studies, single-walled carbon nanotubes (SWCNTs) showed high antibacterial effects [4]. The SWCNTs size play a significant influence in inhibiting several pathogenic microorganisms [4]. Indeed, when the size of the carbon nanomaterials (CNMs) reduced, their surface-to-volume ratio increased, causing a stronger interaction with the microorganisms' cell wall, and therefore a more effective action would be noticed [5]. The association of carbon nanotubes (CNTs) with microbes and the disruption of their metabolic operations, cellular membrane, and morphology were the major reported mechanisms of action [6]. Graphite is a naturally occurring, and crystalline two-dimensional carbon material. Graphene and graphene oxide (G and GO) produce reactive oxygen species (ROS) that leads to physical and chemical oxidation of microorganisms' cell membranes and cell walls, resulting in microbial mortality and reduced resistance [7].

Another relevant topic is the antibacterial properties of CNM composites with biopolymers and NPs such as CuO, Ag, TiO_2, and ZnO, etc. [8,9] However, because of their toxicity, these NPs must be used under standardized precautions [10,11]. Polymers, magnetic NPs, and CNMs can be utilized as carriers or supporters to alleviate this problem, and they can possibly improve the antimicrobial action of the synthesized NPs as well [12]. CNTs, GO, and fullerene nanostructures, in particular, were considered ideal particles for masking the detrimental impacts of NPs [4]. Given their chemical groups and strong dispersion capabilities, CNMs have high functionalization potentials [13]. Synergistic antimicrobial properties are quite essential in the pharmaceutical industry. CNMs, for example, work well with nanoparticles, e.g., CNTs-chitosan, CNTs-Ag [14], GO–Ag [15], C60-ZnO, and C60-CuO [16].

The production procedure had a significant impact on the nanomaterial quality [17]. Arc discharge approaches are known to create nanometals from metal electrodes successfully [18]. Temperature [19], pressure [20,21], electrode shape [18], gap between electrodes [22], current [19], applied voltage [23], type of power supply [23], and dielectric media have a significant impact on the nanoparticle size and shape yields [24].

Toxoplasma gondii is an obligate intracellular pathogenic parasite that can infect all warm-blooded animals (including humans) and induce Toxoplasmosis [25]. The seropositive rates in humans started from 10% to reach over 90%. Ingestion of oocysts (from a cat's faeces or undercooked meat), preceeded by the emergence of sporozoites and bradyzoites from the consumed oocysts. The emerged sporozoites and bradyzoites will penetrate the human intestinal cells, where they will be transformed into tachyzoites [26]. Through the blood or lymphatic system, the tachyzoites will subsequently disseminate to other organs. As a result, tachyzoites can produce an acute (AI) or chronic (CI) infection [27]. During the acute infection stage of the highly virulent RH strain, serum Th1 cytokines (e.g., interleukin (IL)-12, IL-18, interferon (IFN), and tumor necrosis factor (TNF) usually increase, followed by mice mortality after 8 to 10 days post-infection [28]. IL-12, TNF-β, and IFN-α, for example, have been shown to reduce the parasite development (both in vivo and in vitro) [29].

The objective of this research was to find a suitable solution to the increased toxoplasmosis infection hazard. HTADT was used to synthesize Zn, C metal oxides, as well as their composites by combining with multi-walled carbon nanotubes (ZnO-MWCNT), in order to combat *Toxoplasma gondii* infection. This study also aimed to determine the synthesized nanoparticles morphology (using a high-resolution transmission electron microscope HR-TEM), crystallinity (using an X-ray diffraction analyzer XRD), and chemical bonds (using a Fourier transform infrared spectrometer FTIR).

2. Materials and Methods

2.1. Nanoparticles Synthesis

The highly pure Zn and C nanoparticles were synthesized by the arc discharge method according to the designed system shown in Figure 1. As emphasized from Figure 1, the system includes the electrode, alternating current, power supply, voltage employed, vessel capacity, rotating speed, pH, electrode gap, and discharge period. The voltage used was 70 V with an acceptable current of 15 A to ensure a continuous arc discharge to improve the quality and quantity of the nanoparticles. Another important factor was the cylindrical cathode's spinning speed (950 rpm), which accelerated the metal clusters formation and prevented the condensation on the cathode surface. This variable has an important role on particle size characteristics and stability. To increase the yield, the cathode was taken in bigger dimensions in relation to the anode. Then each sample was characterized by using JEOL JEM-2100 high resolution transmission electron microscope (HRTEM, at Alexandria University in Egypt, Model JEOL-JSM-6360LA),, X-ray diffraction analyzer, (JEOL Ltd., Egypt Japan University of Science and Technology, Alexandria, Egypt), and Fourier-transform infrared at (Egypt Japan University of Science and Technology, Alexandria, Egypt).

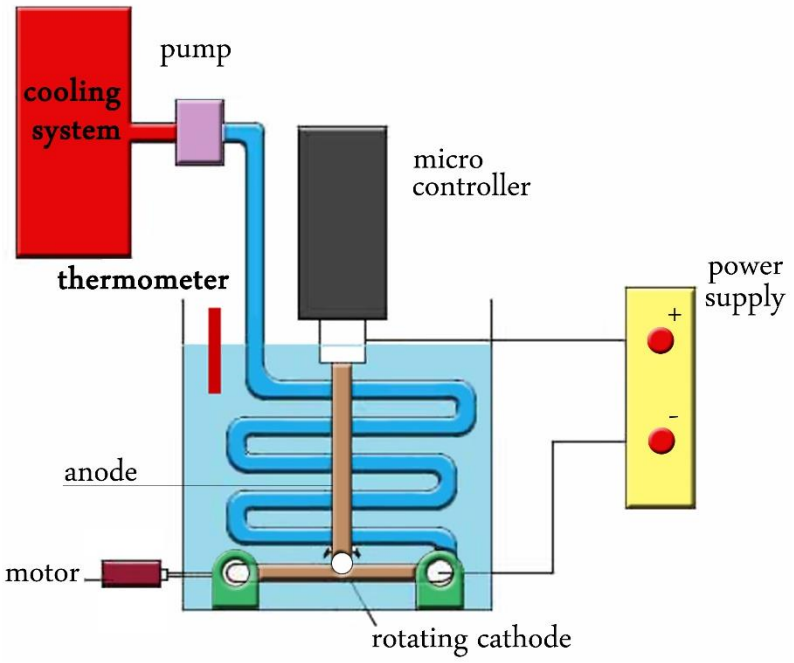

Figure 1. Arc-discharge machine unit.

2.2. Parasite

T. gondii RH virulent strain was maintained in Pharos University in Alexandria by sequential intraperitoneal transmission of tachyzoites (provided from parasitology laboratory, Theodor Bilharz Research Institute, Giza, Egypt) in Swiss Albino mice. Phosphate buffered saline was used to cleanse the peritoneal fluid (PBS). To infect the mice, a portion of the gathered peritoneal fluid was applied to the haemocytometer, and the tachyzoites number was calibrated.

2.3. Drugs Preparation

Animal Grouping and Experimental Design

The study included fifty male Swiss Albino mice that were bred in the lab (6–8 weeks old and 20–25 g weight). The mice were divided into five experimental and control groups (10 mice/group). Except for the uninfected control group mice, each mouse was injected intraperitoneally with the RH strain at a dosage of 2500 tachyzoites/100 µL. The mice were split into the following groups:

- Group I: Negative control, each mouse received 100 µL normal saline for seven days.
- Group II: Positive (Infected untreated) control, each mouse received 100 µL normal saline (the vehicle of the used drugs) orally by gavage needle starting from the day of infection for seven days.
- Group III: Infected mice received 100 µL of ZnO-NPs at a dose of 10 mg/kg/day orally by gavage needle starting from the day of infection for seven days.
- Group IV: Infected mice received 100 µL of GO-NPs at a dose of 10 mg/kg/day orally by gavage needle starting from the day of infection for seven days.
- Group V: Infected mice received 100 µL of ZnO-MWCNT a dose of 10 mg/kg/day orally by gavage needle starting from the day of infection for seven days.

The mice were anaesthetized and sacrificed by cervical dislocation on the 8th day.

For parasitological research, peritoneal exudates, liver, spleen, and brain tissues were collected from all the classified groups, whereas liver, spleen, and brain tissues were gathered and preserved in 10% formalin for histological examination. Each mouse's peritoneal exudate was preserved in glutaraldehyde for morphological examinations with scanning electron microscope (SEM). The mice's blood (5 mL) was taken through the

retro-orbital plexus and centrifuged at 4000 g for 20 min to separate the serum used in inflammatory-marker analyses.

Evaluation of the treatment efficacy:

All the experimental groups were subjected to the following:

2.4. Parasitological Study

2.4.1. Estimation of the Parasite Count

Tachyzoites were enumerated in each Giemsa-stained liver, spleen, and brain impressions. Each mouse's organ was inspected using oil immersion lens, and the mean of ten separate fields was recorded, followed by the mean for each subgroup [30].

Parasite Percent Reduction (%R)

The percentage reductions in the parasite count in the peritoneal exudate, liver, spleen or brain were recorded according to the following Equation (1):

$$\%R = C - E/C \times 10 \quad (1)$$

where %R: Reductions percentage, C: Parasites count in infected untreated group and E: Parasites count in the treated groups [31].

2.4.2. Morphological Study of *T. gondii* Tachyzoites

On the sacrifice day, the peritoneal exudates of all the experimental treated and control groups were collected, fixed in glutaraldehyde, and prepared for SEM examination of the parasites' ultrastructure.

2.5. Inflammatory Biomarkers

Cytokines levels namely (TNF-α, IL-10, IL-6, and IL-1B) in *T. gondii*-infected mouse serum were determined according to the manufacturer's instructions and through the use of enzyme-linked immunosorbent assay (ELISA) kits (R&D Systems, Minneapolis, MN, USA). At 450 nm, the response was measured using a microplate reader (Absorbance 96, Byonoy, Hamburg, Germany) [26].

2.6. Histopathological Study

Specimens from diverse organs (brain, liver, and spleen) were fixated in 10% formalin, dehydrated in successive grades of ethanol, rinsed in xylol, and then imbedded in paraffin wax. Staining of each specimen was utilized by Ehrlich's hematoxylin and eosin (H&E) stain [26].

2.7. Statistical Analyses

Mean ± SD was tabulated for each result. SPSS version 20 was used for the data analysis while ANOVA F-test was used to elaborate the difference between the quantitative variables among experimental groups.

3. Results and Discussion

3.1. Nanoparticles Fabrication

As shown in Figure 2, three different materials were characterized (a) represented MWCNT decorated by Zn-metal, (b) ensured the formation of MWCNT with small diameters, while, (c) & (d) showed GO in nano scale of 5 nm in diameter and 200 nm in length, and (d) & (e) ZnO-NPs displayed hexagonal shape with particle size less than 10 nm.

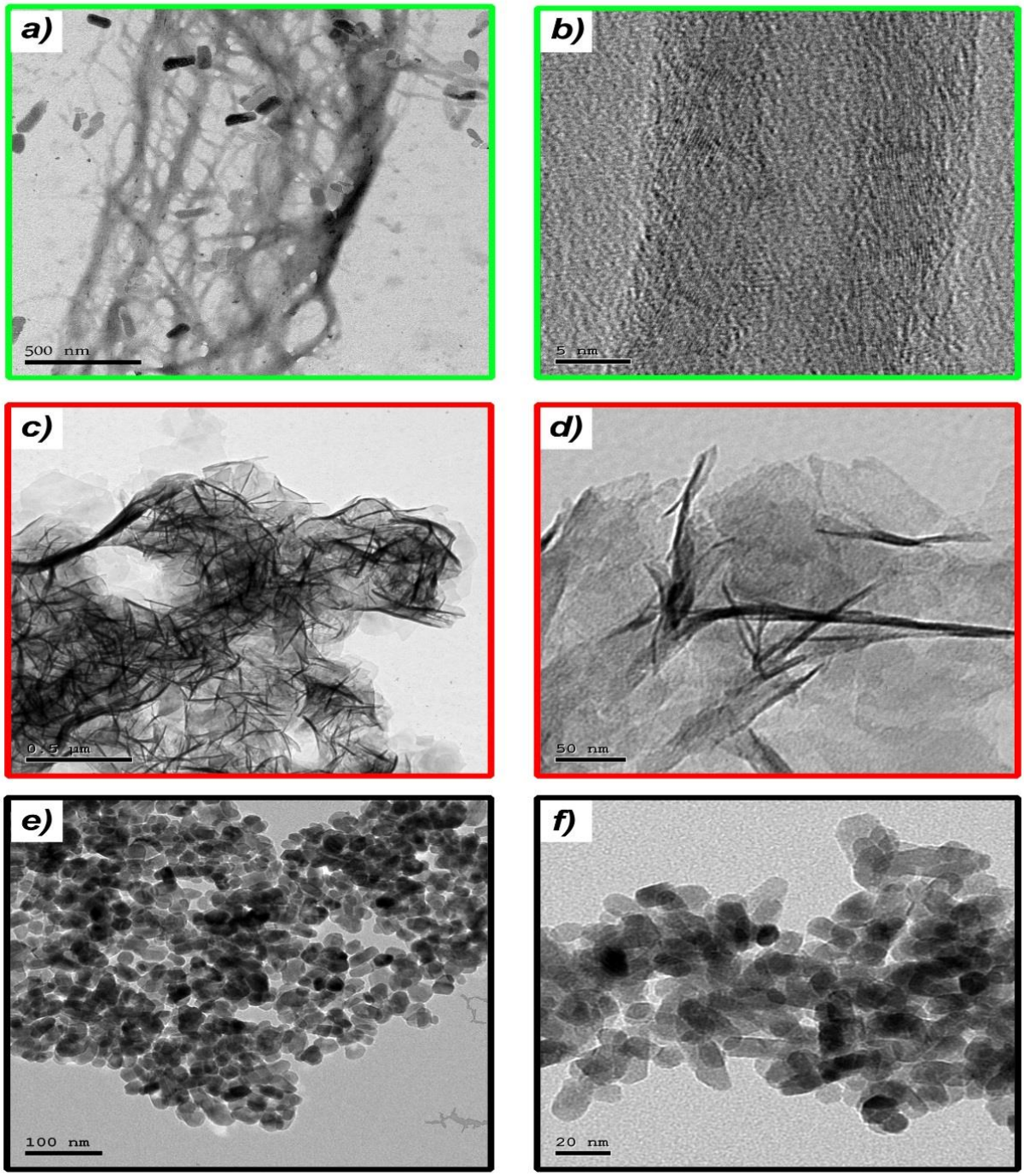

Figure 2. HR-TEM of (**a**) ZnO-MWCNT, (**b**) MWCNT, (**c**,**d**) GO and (**e**,**f**) ZnO.

Figure 2a represented small Zn-NPs size surrounding MWCNT compared with our previous work [32] which may be due to the change of some physical parameters such as rotational speed of the cathode and voltage of power supply [18,33]. On the other hand, Figure 2b showed that MWCNT inner radius was smaller than the previous work despite of their larger outer radius (compared with others).

All nano products were further characterized by XRD as shown in Figure 3a all peaks of nano ZnO were similar to standard diffraction data (JCPDS Card no.; 36–1451), which was combined with two major peaks of MWCNTs at $2\theta = 25.9^\circ$ and $2\theta = 42.37^\circ$ corresponding to the reflection planes (002) & (100), respectively (and were similar to the standard diffraction data (JCPDS Card no.; 01–0646)), which confirmed the formation of

ZnO-MWCNTs. The second diffraction peak displayed in (Figure 3b) showed 2θ = 9.9° in the XRD pattern of graphite oxide samples belonging to the (001) reflection and diffraction peak at 2θ = 42.0° corresponding to (100) to prove the excellent GO synthesis without impurities [34]. It was clear from Figure 3c that the X-Ray diffraction pattern showed 2θ values at 31.84°, 34.52°, 36.38°, 47.64°, 56.7°, 63.06°, 68.1°, and 69.18°. All the mentioned peaks were considered evident peaks indexed as the Zinc oxide wurtzite structure (JCPDS Data Card No: 36-1451) [35].

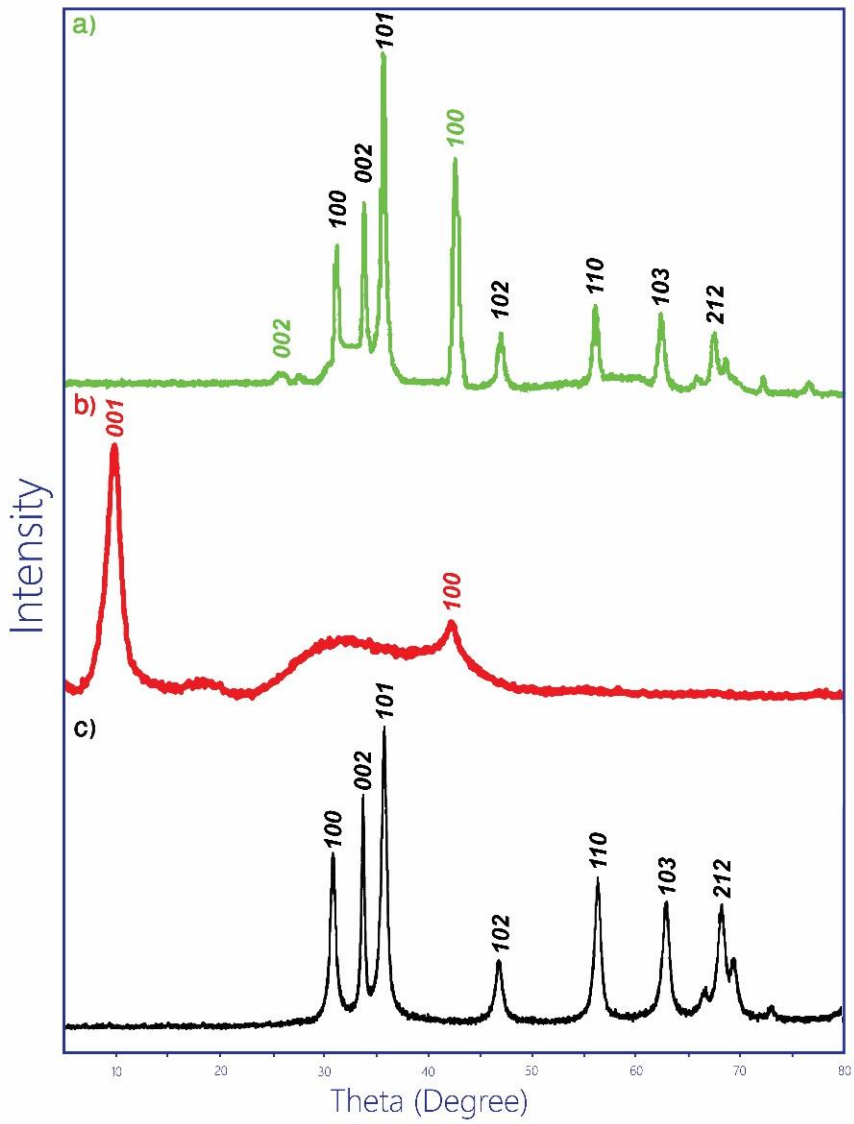

Figure 3. XRD pattern of (**a**) ZnO-MWCNT, (**b**) GO-NPs, and (**c**) ZnO.

FTIR was done for each sample to confirm their chemical bond and to get more information about their structure as shown in Figure 4a representing the ZnO-MWCNT [32], (b) GO-NPs [34], and (c) for ZnO-NPs [36,37]. Each noticed peak in Figure 4 was compared with previous reported values to ensure the chemical structure of the prepared nano materials as tabulated in Table 1.

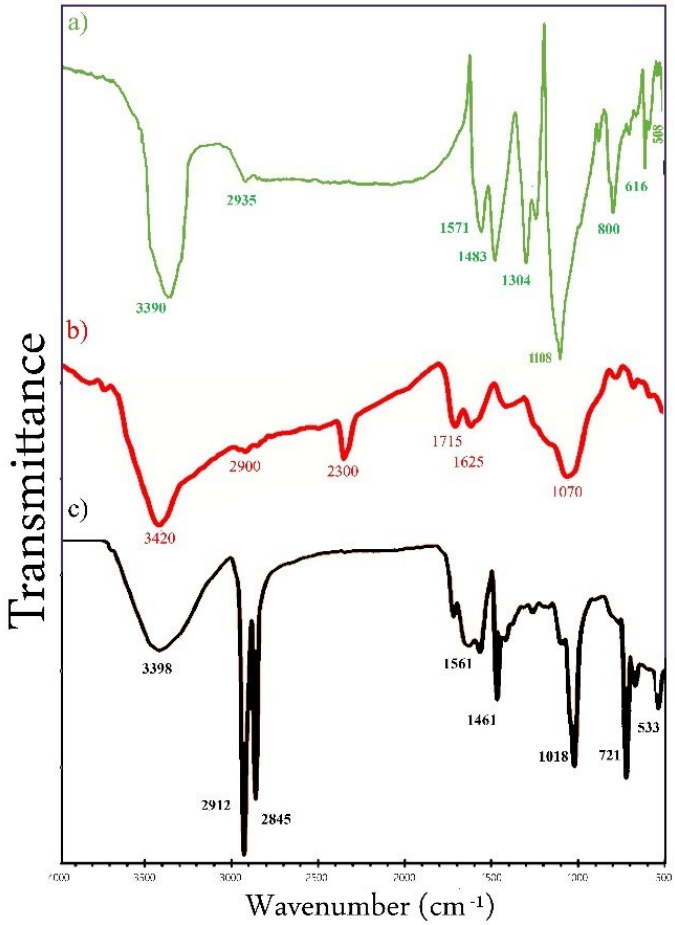

Figure 4. FTIR-analysis for (**a**) ZnO-MWCNT, (**b**) GO, and (**c**) ZnO.

Table 1. Show the results of FTIR for nano products prepared by.

ZnO-MWCNT		GO-NPs		ZnO-NPs	
Frequency (cm^{-1})	**Band Refer to**	**Frequency (cm^{-1})**	**Band Refer to**	**Frequency (cm^{-1})**	**Band Refer to**
3390	-OH	3420	-OH	3398	-OH group
2935	-C=H			2912	-C=H
1571	-C=C	2900	-C=H	2845	-OH group
1483	-C-H	2300		1561	-C=C
1304	-OH	1715	-C=O	1461	-C=O
1108	-C=O			1018	-C=O
800	-C-H	1625	-C=C	721	Zn-O
616	Zn-O			533	Zn-O
508	Zn-O	1070	-C-C		

3.2. Parasitological Study

3.2.1. Parasite Count and Percent Reduction (%R)

The mean tachyzoites count in all groups revealed that the parasite count reduction in liver was the highest compared to other organs with percent reduction in parasite count reached 41, 27 and 52% for groups III, IV, and V respectively (statistically significant difference compared to the infected untreated group).

There was a statistically significant reduction in parasite count in all treated groups and infected untreated group in all organs (Table 2, Figure 5). As for treated mice, the lowest mean tachyzoites count and the highest percent reduction were detected in mice receiving ZnO-MWCNT in all the tested organs.

Table 2. The parasite count and the percentage reduction in the organs of RH infected mice.

Groups		Liver (n = 10)	Spleen (n = 10)	Brain (n = 10)
Group II a	Mean ± SD	16.7 ± 0.67 [b,c,d]	9.7 ± 0.67 [b,c,d]	2.8 ± 0.60 [b,c,d]
Group III	Mean ± SD R1%	9.9 ± 0.9 [a,c,d] 41	6.1 ± 0.99 [a,c] 37	1.3 ± 0.46 [a,c] 54
Group IV	Mean ± SD R2%	12.2 ± 1.14 [a,b,d] 27	7.6 ± 0.97 [a,b,d] 22	2 ± 0.45 [a,b] 29
Group V	Mean ± SD R3%	8 ± 1.05 [a,b,c] 52	5.3 ± 0.82 [a,c] 45	1.1± 0.54 [a,c] 61
	F p	146.1 <0.001	48.1 <0.001	20.2 <0.001

[a] Significant with subgroup II; [b] Significant with subgroup III; [c] Significant with subgroup IV; [d] Significant with subgroup V.

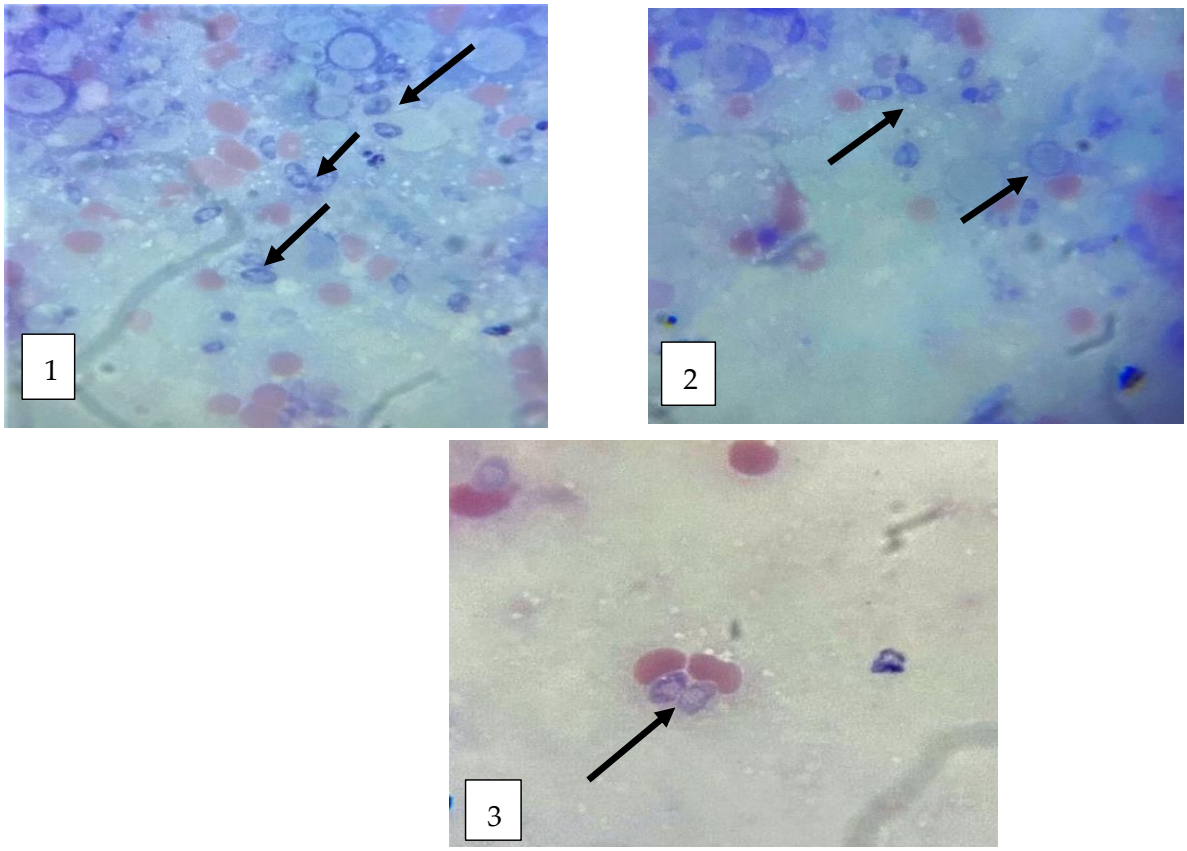

Figure 5. *T. gondii* tachyzoites of infected mice treated with ZnO-MWCNT in Giemsa-stained liver (**1**), Spleen (**2**) and brain (**3**) impression smear, × 1000.

These results were inconsistent with previous study that showed that ZnO-NPs had considerable prophylactic benefits against chronic toxoplasmosis in mice, with oral treatment of ZnNPs at dosages of 32.5, 75, and 150 mg/kg that led to reducing the parasite burden and even controlling the toxoplasmosis infection totally. These findings demonstrated that ZnNPs boosted the innate immune system, which might explain their potent preventive effects [38]. On the contrary, Swedin [39] reported that SWCNT did not affect the *T. gondii* parasitic count in the various tested organs in comparison to the infected untreated mice group.

GII: RH infected control group, GIII: infected group received ZnO-NPs, GIV: infected group received GO-NPs, GV: infected group received ZnO-MWCNT. R1 percentage of

reduction in infected group taken ZnO-NPs, R2 percentage of reduction in infected group taken GO-NPs, R3 percentage of reduction in infected group taken ZnO-MWCNT. *n*: initial number of mice in the subgroup, SD: standard deviation, F: F test (ANOVA) and $p \leq 0.05$ (statistically significant).

3.2.2. Morphological Study of *T. gondii* Tachyzoites

Scanning electron microscopic study showed normal smooth surfaces of *T. gondii* tachyzoites collected from the peritoneal exudates of infected untreated mice. While, tachyzoites from treated groups showed complete distortion in the parasite surface (Figure 6). SEM micrographs with different magnification were added as Supplementary Data (Figure S1).

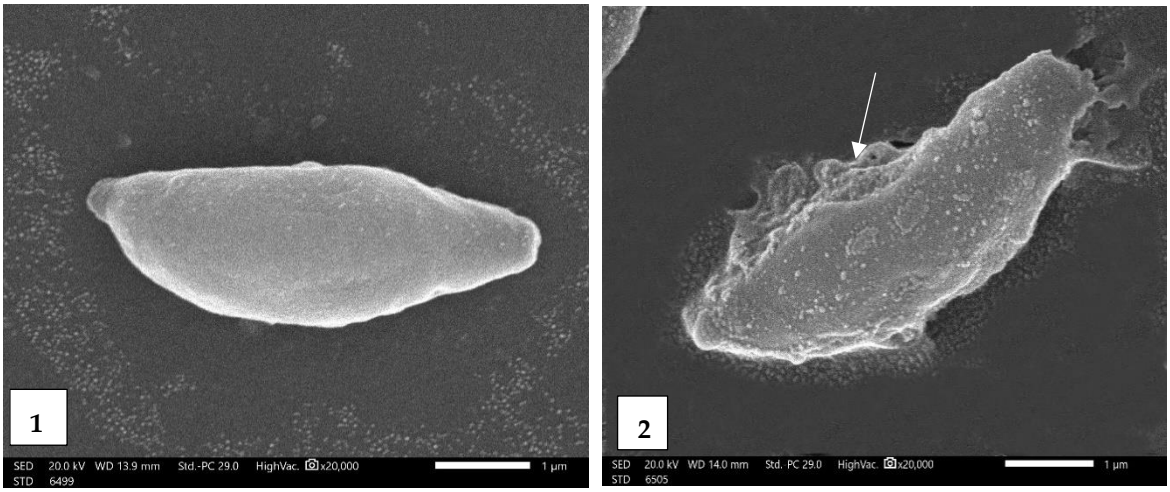

Figure 6. SEM of *Toxoplasma gondii* tachyzoite in infected untreated control group showing completely regular smooth surface (**1**) (×20,000) and (**2**) A SEM of *Toxoplasma gondii* tachyzoite in infected group showing completely irregular surface, multiple ridges, irregular papules, and dimples (arrow) (×20,000).

3.3. Inflammatory and Anti-Inflammatory Cytokines in Infected and Treated Groups

Inflammatory and anti-inflammatory cytokines (TNF-α, IL-10, IL-6, and IL-1B) assessments were used to evaluate the inflammatory processes in response to *T. gondii* infection and the used treatments. According to Hwang et al. [29], *T. gondii* acute infection resulting in an increased inflammatory and anti-inflammatory cytokine expressions, as well as activation and proliferation of microglial cells. Table 3 proved that the inflammatory and anti-inflammatory cytokine concentrations were notably higher in infected untreated mice, which indicated the progression of the acute infection (AI). Group V (ZnO-MWCNT treated group) showed an impressive reduced inflammatory response and cytokine concentrations that were reliably close to those of healthy (uninfected) mice. Hojyo and Fukada [40] mentioned that the anti-inflammatory cytokines such as interleukins of IL-1b, IL-6, and tumor necrosis factor alpha (TNF-α) were affected by zinc nanoparticles remedy. It also played a major role in distinguishing natural killer cells (NK cells) from major histocompatibility (MHC) class 1 primary cells. Zinc (Zn) is also necessary for the proper balance of T cell subsets. On the other hand, Swedin et al. [39] declared that pre-exposure to SWCNT does not enhance or suppress the early immune response to *T. gondii* in mice.

Table 3. Inflammatory response of the infected and non-infected mice groups.

Mice Groups	TNF-α (ng/mL)	IL-10 (ng/mL)	IL-6 (pg/mL)	IL-1β (ng/mL)
Group I (Normal)	1.91 ± 0.41	1.32 ± 0.19	395.43 ± 0.82	1.45 ± 0.52
Group II (Infected untreated)	3.23 ± 0.58	2.36 ± 0.25	637.90 ± 0.29	11.24 ± 0.33
Group III (ZnO)	2.03 ± 1.07	1.65 ± 0.31	539.83 ± 1.03	9.43 ± 0.97
Group IV (GO)	2.60 ± 0.27	2.11 ± 0.22	548.64 ± 0.30	7.47 ± 0.29
Group V (ZnO-MWCNT)	2.00 ± 0.38	1.49 ± 0.93	450.80 ±0.64	6.12 ± 0.83

3.4. Histopathological Studies

3.4.1. Brain

Microscopic examination of H&E stained cerebral cortex sections from the frontal area of Group I (control) revealed the cerebral cortex's well-known normal structure. Neurons, notably pyramidal and granule cells, as well as neuroglial cells, were abundant inside these layers. The neuropil, a pink-stained background, was a tangle of neuronal and glial cells.

When the infected untreated group was investigated, it revealed significant multifocal histological abnormalities in the cerebellum when compared to the control healthy group. As a result of the parasitic infection, many vacuoles of varied sizes grew between and inside many cells in all the cerebellum layers, resulting in a huge cerebral infract.

Compared to the previous results, the treated groups (III and IV) showed an improvement in brain histological features and decreased number of vacuoles and few unconnected cerebral infracts. The lower the number of cerebral infracts, the better the therapy, as seen in the ZnO-NPs-treated group in comparison to the GO-NPs-treated group.

Cerebral examination of the ZnO-MWCNT-treated group revealed that a small number of vacuoles had vanished. It also revealed typical neuron architecture with central big vesicular nuclei having one or more nucleoli diffusing in spongy matrix, as well as peripheral dispersion of Nissl granules suggesting the synergistic impact of ZnO nanoparticles and carbon nanotubes (Figure 7).

3.4.2. Liver

H&E stained samples of the control group's liver exhibited normal hepatic architecture with a minor dilated central vein.

On the other hand, the liver sector of the infected untreated group displayed dilated central veins and congested hepatic sinusoids, making the liver seemed more perforated. The cytoplasm of certain hepatocytes was vacuolated. Furthermore, minor multifocal infiltrations of inflammatory cells were seen between hemorrhage regions, accompanied by unclear cell borders.

The treated groups improved the histopathological results significantly, as evidenced by decreased congestion of blood sinusoids in the GO-NPs-treated group with cellular infiltration. In addition, the ZnO-NPs-treated group had a substantial decrease in the number of clogged blood sinusoids, indicating the higher efficacy of zinc oxide than graphite in the hepatocytes.

Furthermore, the results of Group 5 demonstrated maintained hepatic architecture. Hepatocytes were distributed in a radial pattern from central veins, with rounded vesicular nuclei centrally positioned and divided by blood sinusoids. There was still some dilation in the central vein. There were no necrotic foci found (Figure 7).

3.4.3. Spleen

The splenic architecture of the control group was described as clearly demarcated white and red pulp with continuous trabecular throughout the tissues. The typical pattern of periarteriolar lymphoid sheaths (PALS) and lymphoid follicles was also seen in the white pulp.

The infected untreated group revealed big, clogged blood vessels as an indication of spleen injury, which was followed by tissue degeneration. Moreover, the borders between regions of white pulp and red pulp weren't totally observed, which was crucial evidence of the damage degree.

Some symptoms of inflammation were observed in the GO-NPs-treated group, which was concerning output considering the pro-inflammatory boost of the pancreatic white pulp (producing inflammatory mediators). Furthermore, blood vessel congestion remained noticeable. The traditional borders between the WP segments were gradually eroding.

Both groups IV and V showed normal patterns of red and white palp with normal marginal zone and lymphatic follicles, comparable to the control group.

The most surprising observation was the non-significant difference between the ZnO-NPs-treated group and the ZnO-MWCNT-treated group, which has crucial scientific implications, which may be explained by the fact that graphite nanoparticles have little or no impact on the splenic tissue (Figure 7). Other photomicrographs were added as a Supplementary Data (Figure S2).

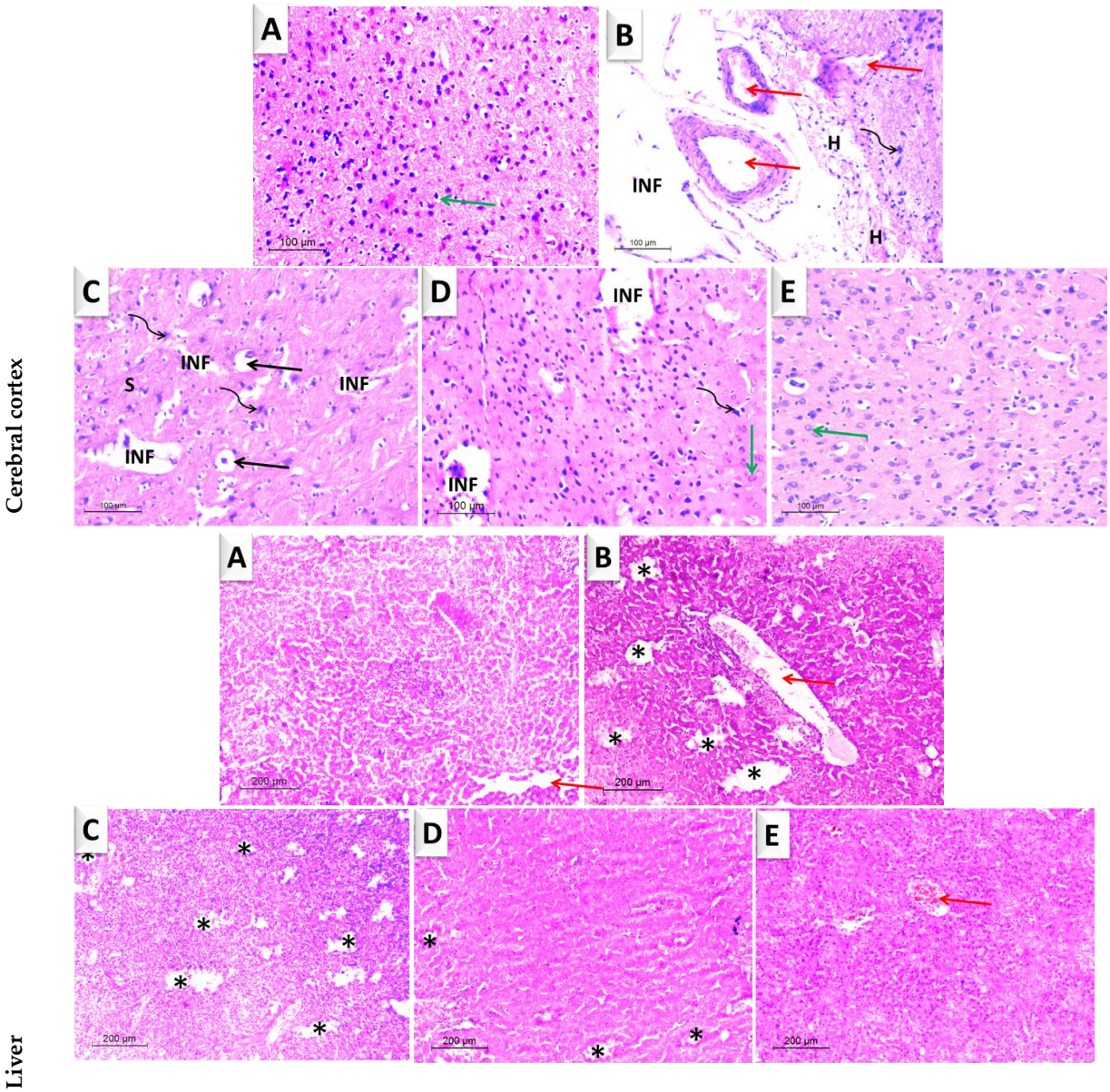

Figure 7. *Cont.*

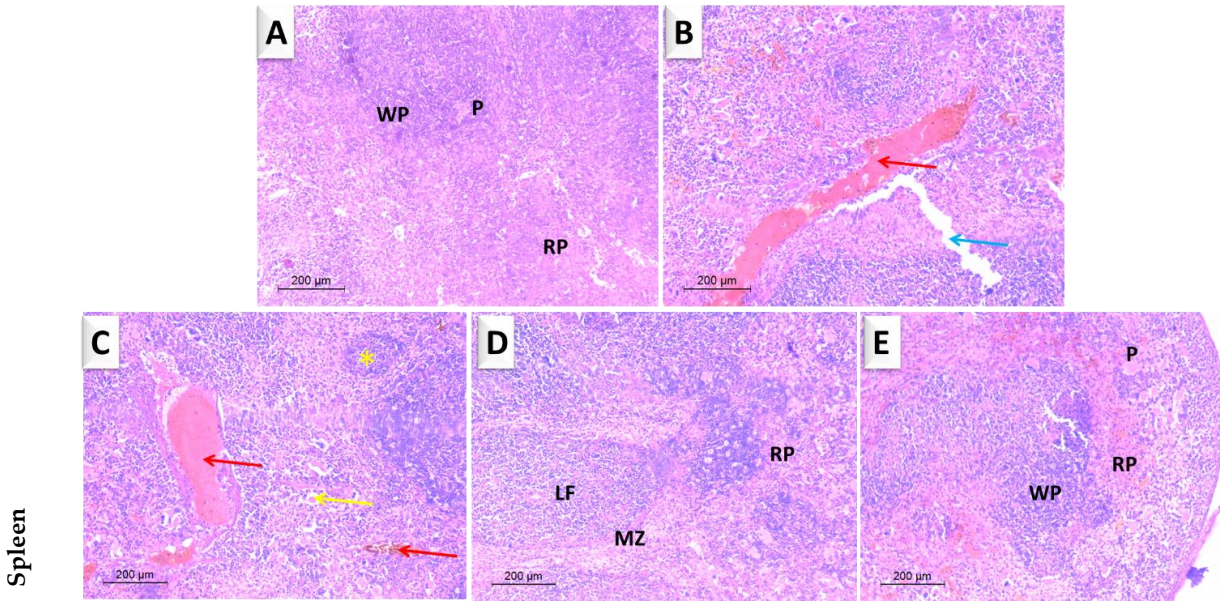

Figure 7. A photomicrograph illustrates several H&E-stained tissue specimens from the cerebral cortex, liver, and spleen. (**A**); Group I healthy control (**B**); Group II infected control (**C**); Group III received Zn-NPs (**D**); Group IV received GO-NPs (**E**): Group V received ZnO-MWCNT. Note: Red arrow refers to blood vessel, Green arrows refer to normal neuron, INF: cerebral infract, S: spongy matrix, H: hemorrhage, Bent black arrow: necrotic neurons, Black arrows: perivascular neurons, Black stars refer to dilated blood sinusoids, Blue arrow: cellular degeneration, RP: red Pulp, WP: white Pulp, LF: Lymphoid follicle, MZ marginal zone, P: periarteriolar lymphocyte sheath, Yellow arrow: cellular vacuole and Yellow star: Small lymphoid follicle.

4. Conclusions

The well-dispersed multi-walled carbon nanotubes lined with ZnO (ZnO-MWCNT), graphene oxide (GO-NPs), and zinc oxide (ZnO-NPs) were successfully synthesized through the arc discharge method. The formed nanoparticles were characterized by transmission electron microscope, IR and XRD analyses which ensured the formation of ZnO-MWCNT with small diameters. This is the first work to assess the antiparasitic effect of the synthesized ZnO-MWCNT against *Toxoplasma gondii* infection in mice. The lowest mean tachyzoites count in all the tested organs was observed in mice received ZnO-MWCNT. *T. gondii* infection resulted an increased level of inflammatory cytokines, as well as activation and proliferation of microglial cells while ZnO-MWCNT-treated group showed a significant reduction and regulation of the tested cytokines. Histopathological study of ZnO-MWCNT-treated group revealed almost normal cell architecture, which proved the ZnO-MWCNT efficacy and safety.

Supplementary Materials: The following supporting information can be downloaded at: https://www.mdpi.com/article/10.3390/met12081246/s1, Figure S1: SEM of *Toxoplasma gondii* tachyzoite in infected group showing completely irregular surface, multiple ridges, irregular papules and dimples (X 10,000; Figure S2: A photomicrograph illustrates several H&E-stained tissue specimens from the cerebral cortex, liver, and spleen. (A); Group I healthy control (B); Group II infected control (C); Group III received Zn-NPs (D); Group IV received GO-NPs (E): Group V received ZnO-MWCNT. Note: Grey arrow: nuclear degeneration, Black insert: necrosis, Red arrow refers to blood vessel, INF: cerebral infract, Blue arrow: cellular degeneration, Black stars refer to dilated blood sinusoids, RP: red Pulp, WP: white Pulp and LF: Lymphoid follicle.

Author Contributions: Conceptualization E.A.M.; methodology, B.A.B., B.H.E., M.E.-K., E.A.M., M.H. and J.Y.A.-H.; software, M.E.-K.; validation, B.A.B., B.H.E., M.E.-K. and E.A.M.; writing—original draft preparation, B.A.B., B.H.E., M.E.-K., E.A.M. and M.H.; writing—review and editing, B.A.B.,

B.H.E., M.E.-K. and E.A.M.; visualization, B.H.E.; project administration, J.Y.A.-H.; funding acquisition, J.Y.A.-H. All authors have read and agreed to the published version of the manuscript.

Funding: The research was funded by Princess Nourah bint Abdulrahman University Researchers Supporting Project number (PNURSP2022R24), Princess Nourah bint Abdulrahman University, Riyadh, Saudi Arabia.

Institutional Review Board Statement: This work was approved by the ethics committee of Faculty of Science, Alexandria University.

Informed Consent Statement: Not applicable.

Data Availability Statement: All the original data are available upon reasonable request for correspondence authors.

Conflicts of Interest: The authors declare no conflict of interest.

References

1. Shoukat, R.; Khan, M.I. Carbon nanotubes: A review on properties, synthesis methods and applications in micro and nanotechnology. *Microsyst. Technol.* **2021**, *27*, 4183–4192. [CrossRef]
2. Kamedulski, P.; Kaczmarek-Kedziera, A.; Lukaszewicz, J.P. Influence of intermolecular interactions on the properties of carbon nanotubes. *Bull. Mater. Sci.* **2018**, *41*, 76. [CrossRef]
3. Kamedulski, P.; Gauden, P.A.; Lukaszewicz, J.P.; Ilnicka, A. Effective Synthesis of Carbon Hybrid Materials Containing Oligothiophene Dyes. *Materials* **2019**, *12*, 3354. [CrossRef] [PubMed]
4. Azizi-Lalabadi, M.; Hashemi, H.; Feng, J.; Jafari, S.M. Carbon nanomaterials against pathogens; the antimicrobial activity of carbon nanotubes, graphene/graphene oxide, fullerenes, and their nanocomposites. *Adv. Colloid Interface Sci.* **2020**, *284*, 102250. [CrossRef] [PubMed]
5. Su, Q.; Gan, L.; Liu, J.; Yang, X. Carbon dots derived from pea for specifically binding with Cryptococcus neoformans. *Anal. Biochem.* **2020**, *589*, 113476. [CrossRef] [PubMed]
6. Ji, H.; Sun, H.; Qu, X. Antibacterial applications of graphene-based nanomaterials: Recent achievements and challenges. *Adv. Drug Deliv. Rev.* **2016**, *105*, 176–189. [CrossRef] [PubMed]
7. Xie, Y.Y.; Hu, X.H.; Zhang, Y.W.; Wahid, F.; Chu, L.Q.; Jia, S.R.; Zhong, C. Development and antibacterial activities of bacterial cellulose/graphene oxide-CuO nanocomposite films. *Carbohydr. Polym.* **2020**, *229*, 115456. [CrossRef] [PubMed]
8. Azizi-Lalabadi, M.; Ehsani, A.; Divband, B.; Alizadeh-Sani, M. Antimicrobial activity of Titanium dioxide and Zinc oxide nanoparticles supported in 4A zeolite and evaluation the morphological characteristic. *Sci. Rep.* **2019**, *9*, 17439. [CrossRef]
9. Azizi-Lalabadi, M.; Alizadeh-Sani, M.; Khezerlou, A.; Mirzanajafi-Zanjani, M.; Zolfaghari, H.; Bagheri, V.; Divband, B.; Ehsani, A. Nanoparticles and Zeolites: Antibacterial Effects and their Mechanism against Pathogens. *Curr. Pharm. Biotechnol.* **2019**, *20*, 1074–1086. [CrossRef]
10. De Jong, W.H.; De Rijk, E.; Bonetto, A.; Wohlleben, W.; Stone, V.; Brunelli, A.; Badetti, E.; Marcomini, A.; Gosens, I.; Cassee, F.R. Toxicity of copper oxide and basic copper carbonate nanoparticles after short-term oral exposure in rats. *Nanotoxicology* **2019**, *13*, 50–72. [CrossRef]
11. Yu, Z.; Wang, W.; Kong, F.; Lin, M.; Mustapha, A. Cellulose nanofibril/silver nanoparticle composite as an active food packaging system and its toxicity to human colon cells. *Int. J. Biol. Macromol.* **2019**, *129*, 887–894. [CrossRef] [PubMed]
12. Prucek, R.; Tuček, J.; Kilianová, M.; Panáček, A.; Kvítek, L.; Filip, J.; Kolář, M.; Tománková, K.; Zbořil, R. The targeted antibacterial and antifungal properties of magnetic nanocomposite of iron oxide and silver nanoparticles. *Biomaterials* **2011**, *32*, 4704–4713. [CrossRef] [PubMed]
13. Dreyer, D.R.; Park, S.; Bielawski, C.W.; Ruoff, R.S. The chemistry of graphene oxide. *Chem. Soc. Rev.* **2010**, *39*, 228–240. [CrossRef] [PubMed]
14. Xia, L.; Xu, M.; Cheng, G.; Yang, L.; Guo, Y.; Li, D.; Fang, D.; Zhang, Q.; Liu, H. Facile construction of Ag nanoparticles encapsulated into carbon nanotubes with robust antibacterial activity. *Carbon* **2018**, *130*, 775–781. [CrossRef]
15. Cobos, M.; De-La-Pinta, I.; Quindós, G.; Fernández, M.J.; Fernández, M.D. Synthesis, physical, mechanical and antibacterial properties of nanocomposites based on poly (vinyl alcohol)/graphene oxide–silver nanoparticles. *Polymers* **2020**, *12*, 723. [CrossRef]
16. Zhao, L.; Ji, Y.; Sun, P.; Li, R.; Xiang, F.; Wang, H.; Yang, Y. Effects of individual and complex ciprofloxacin, fullerene C60, and ZnO nanoparticles on sludge digestion: Methane production, metabolism, and microbial community. *Bioresour. Technol.* **2018**, *267*, 46–53. [CrossRef]
17. El-Khatib, A.M.; Elsafi, M.; Sayyed, M.; Abbas, M.; El-Khatib, M. Impact of micro and nano aluminium on the efficiency of photon detectors. *Results Phys.* **2021**, *30*, 104908. [CrossRef]
18. El-Khatib, A.M.; Badawi, M.S.; Ghatass, Z.F.; Mohamed, M.M.; Elkhatib, M. Synthesize of Silver Nanoparticles by Arc Discharge Method Using Two Different Rotational Electrode Shapes. *J. Clust. Sci.* **2018**, *29*, 1169–1175. [CrossRef]

19. Timerkaev, B.A.; Shakirov, B.R.; Timerkaeva, D.B. Creation of Silicon Nanostructures in Electric Arc Discharge. *High Energy Chem.* **2019**, *53*, 162–166. [CrossRef]
20. Zhao, T.; Liu, Y.; Zhu, J. Temperature and catalyst effects on the production of amorphous carbon nanotubes by a modified arc discharge. *Carbon* **2005**, *43*, 2907–2912. [CrossRef]
21. Su, Y.; Yang, Z.; Wei, H.; Kong, E.S.-W.; Zhang, Y. Synthesis of single-walled carbon nanotubes with selective diameter distributions using DC arc discharge under CO mixed atmosphere. *Appl. Surf. Sci.* **2011**, *257*, 3123–3127. [CrossRef]
22. Biró, L.; Horváth, Z.; Szalmás, L.; Kertész, K.; Wéber, F.; Juhász, G.; Radnóczi, G.; Gyulai, J. Continuous carbon nanotube production in underwater AC electric arc. *Chem. Phys. Lett.* **2003**, *372*, 399–402. [CrossRef]
23. Arora, N.; Sharma, N. Arc discharge synthesis of carbon nanotubes: Comprehensive review. *Diam. Relat. Mater.* **2014**, *50*, 135–150. [CrossRef]
24. Tseng, K.-H.; Lin, Y.-S.; Ku, H.-C.; Lee, H.-L. Study on the Characteristics of Zinc Oxide Nanocolloid Prepared Using Electrical Spark Discharge Method. *J. Clust. Sci.* **2021**, *33*, 145–150. [CrossRef]
25. Dubey, J.P.; Hotea, I.; Olariu, T.R.; Jones, J.L.; Darabus, G. Epidemiological review of toxoplasmosis in humans and animals in Romania. *Parasitology* **2014**, *141*, 311–325. [CrossRef]
26. Almutairi, T.M.; Rezki, N.; Aouad, M.R.; Hagar, M.; Bakr, B.A.; Hamed, M.T.; Moneer, E.A. Exploring the Antiparasitic Activity of Tris-1, 3, 4-Thiadiazoles against Toxoplasma gondii-Infected Mice. *Molecules* **2022**, *27*, 2246. [CrossRef]
27. Wohlfert, E.A.; Blader, I.J.; Wilson, E.H. Brains and Brawn: Toxoplasma Infections of the Central Nervous System and Skeletal Muscle. *Trends Parasitol.* **2017**, *33*, 519–531. [CrossRef]
28. Mordue, D.G.; Monroy, F.; La Regina, M.; Dinarello, C.A.; Sibley, L.D. Acute Toxoplasmosis Leads to Lethal Overproduction of Th1 Cytokines. *J. Immunol.* **2001**, *167*, 4574–4584. [CrossRef]
29. Hwang, Y.S.; Shin, J.-H.; Yang, J.-P.; Jung, B.-K.; Lee, S.H.; Shin, E.-H. Characteristics of Infection Immunity Regulated by Toxoplasma gondii to Maintain Chronic Infection in the Brain. *Front. Immunol.* **2018**, *9*, 158. [CrossRef]
30. Thiptara, A.; Kongkaew, W.; Bilmad, U.; Bhumibhamon, T.; Anan, S. Toxoplasmosis in piglets. *Ann. Acad. Sci.* **2006**, *1081*, 336–338. [CrossRef]
31. Penido, M.L.D.O.; Nelson, D.L.; Vieira, L.; Coelho, P.M.Z. Schistosomicidal activity of alkylaminooctanethiosulfuric acids. *Memórias Inst. Oswaldo Cruz* **1994**, *89*, 595–602. [CrossRef] [PubMed]
32. El-Khatib, A.; Bondouk, I.; Omar, K.; Hamdy, A. Impact of changing electrodes dimensions and different ACs on the characteristics of nano composites NZnO/MWCNTs prepared by the arc discharge method. *Surf. Interfaces* **2022**, *29*, 101736. [CrossRef]
33. Aljohani, F.S.; Elsafi, M.; Ghoneim, N.I.; Toderaş, M.; Sayyed, M.I.; Mohafez, H.; Islam, M.A.; Khandaker, M.U.; El-Khatib, M. Water Treatment from MB Using Zn-Ag MWCNT Synthesized by Double Arc Discharge. *Materials* **2021**, *14*, 7205. [CrossRef] [PubMed]
34. Titelman, G.; Gelman, V.; Bron, S.; Khalfin, R.; Cohen, Y.; Bianco-Peled, H. Characteristics and microstructure of aqueous colloidal dispersions of graphite oxide. *Carbon* **2005**, *43*, 641–649. [CrossRef]
35. Bigdeli, F.; Morsali, A.; Retailleau, P. Syntheses and characterization of different zinc(II) oxide nano-structures from direct thermal decomposition of 1D coordination polymers. *Polyhedron* **2010**, *29*, 801–806. [CrossRef]
36. Khalil, A.M.; El-Khatib, A.M.; El-Khatib, M. Synthesis of hexagonal nanozinc by arc discharge for antibacterial water treatment. *Surf. Innov.* **2019**, *8*, 165–171. [CrossRef]
37. El-Khatib, A.M.; Yousef, N.; Ghatass, Z.; Badawi, M.S.; Mohamed, M.; Elkhatib, M. Synthesized Silver Carbon Nanotubes and Zinc Oxide Nanoparticles and their Ability to Remove Methylene Blue Dye. *J. Nano Res.* **2019**, *56*, 1–16. [CrossRef]
38. Saadatmand, M.; Al-Awsi, G.R.L.; Alanazi, A.D.; Sepahvand, A.; Shakibaie, M.; Shojaee, S.; Mohammadi, R.; Mahmoudvand, H. Green synthesis of zinc nanoparticles using Lavandula angustifolia Vera. Extract by microwave method and its prophylactic effects on Toxoplasma gondii infection. *Saudi J. Biol. Sci.* **2021**, *28*, 6454–6460. [CrossRef]
39. Swedin, L.; Arrighi, R.; Andersson-Willman, B.; Murray, A.; Chen, Y.; Karlsson, M.C.I.; Georén, S.K.; Tkach, A.V.; Shvedova, A.A.; Fadeel, B.; et al. Pulmonary exposure to single-walled carbon nanotubes does not affect the early immune response against Toxoplasma gondii. *Part. Fibre Toxicol.* **2012**, *9*, 16. [CrossRef]
40. Hojyo, S.; Fukada, T. Roles of Zinc Signaling in the Immune System. *J. Immunol. Res.* **2016**, *2016*, 6762343. [CrossRef]